ADVANCED ENERGY MATERIALS
www.advenergymat.de

Ligand-Mediated Self-Terminating Growth of Single-Atom Pt on Au Nanocrystals for Improved Formic Acid Oxidation Activity

Moxuan Liu, Zhaojun Liu, Miao Xie, Zhixue Zhang, Shumeng Zhang, Tao Cheng, and Chuanbo Gao**

Decreasing the ensemble size of Pt to isolated single atoms is the key to enhance the electrocatalytic formic acid oxidation reaction (FAOR) by bypassing the indirect reaction path that involves the poisoning by the CO intermediate. However, it is challenging to construct isolated Pt single atoms on a foreign metal substrate, especially at high Pt loadings, because Pt tends to form large ensembles due to the high Pt–Pt bond energy. Herein, a ligand-mediated self-terminating growth strategy is reported for reliably controlling the ensemble size of Pt on an Au substrate. The key is to introduce a ligand of sulfite (SO_3^{2-}) into the synthesis, which preferentially adsorbs at Pt sites, thus substantially increasing the kinetic barrier toward Pt–Pt bond formation. This strategy enables reliable formation of isolated Pt single atoms even at high Pt loadings (up to 26% coverage on Au), which is difficult to achieve by regular syntheses. The resulting catalyst exhibits a high FAOR activity of 38.6 A mg_{Pt}^{-1} in 0.5 M H_2SO_4+0.25 M HCOOH, 370 times greater than that of the commercial Pt/C. It is believed this strategy is general and potentially applicable to the fabrication of a wide range of noble metal catalysts with tailored ensemble sizes for energy conversion.

1. Introduction

Designing highly efficient catalysts for fuel cells is an effective way to solve the resource shortage problem.[1–4] The ensemble size of noble metals plays a critical role in electrocatalytic formic acid oxidation reaction (FAOR) and many other important heterogeneous catalytic reactions.[5–13] A dual-path mechanism has been proposed for the FAOR based on experiments and theory, i.e., a direct path that involves the dehydrogenation of HCOOH directly to CO_2, and an indirect path that involves the dehydration of HCOOH to CO_2 via a poisoning intermediate of CO.[5–8] The direct path is preferred because it bypasses the formation of CO that easily poisons the catalyst. It is recognized that the reaction paths of the FAOR can be effectively regulated by the ensemble size of the Pt catalyst. The direct and indirect paths of the FAOR occur at isolated single atoms and large ensembles of Pt, respectively.[5–8] Therefore, Pt catalysts with the smallest ensemble size, i.e., isolated single atoms, are among the most active catalysts for this reaction.

However, it is difficult to reliably construct isolated single atoms of Pt on a foreign metal substrate in a wet-chemical synthesis, because the formation of large ensembles or islands of Pt is an energetically more favorable process owing to the high Pt–Pt bond energy.[14–17] It is only possible to maintain isolated single atoms of Pt at an early stage of the Pt growth when the Pt loading is very low on the substrate. For example, an Au@Pt core–shell structure showed excellent FAOR activity only when the number of the Pt layers on the Au substrate was <0.1, i.e., the coverage of Pt on the Au substrate was <10%.[18] Unfortunately, the substrates for the growth of Pt are usually noble metals as well, e.g., Au, to avoid any galvanic replacement reaction in the synthesis and oxidative etching in the electrocatalysis. The sparse dispersion of Pt on these noble metal substrates significantly increases the cost of the catalysts and impedes their wide applications.

There have been electrochemical methods that can control the ensemble size of noble metals such as Pt on foreign substrates by taking advantage of the underpotential deposition (UPD) phenomenon.[19–24] Metal atoms such as Cu and Pb form a full atomic layer on a noble metal substrate, due to the UPD, which are then substituted by Pt through the galvanic replacement reaction, leading to the formation of a (sub-)monolayer Pt atoms on the noble metal substrate.[19–22] Another approach utilizes the UPD of H to achieve the self-terminating growth of

M. Liu, Z. Liu, Z. Zhang, S. Zhang, C. Gao
Center for Materials Chemistry
Frontier Institute of Science and Technology
and State Key Laboratory of Multiphase Flow in Power Engineering
Xi'an Jiaotong University
Xi'an, Shaanxi 710054, China
E-mail: gaochuanbo@mail.xjtu.edu.cn
M. Xie, T. Cheng
Institute of Functional Nano & Soft Materials (FUNSOM)
Jiangsu Key Laboratory for Carbon-Based Functional Materials & Devices
Joint International Research Laboratory of Carbon-Based Functional Materials and Devices
Soochow University
Suzhou, Jiangsu 215123, China
E-mail: tcheng@suda.edu.cn
The ORCID identification number(s) for the author(s) of this article can be found under https://doi.org/10.1002/aenm.202103195.

DOI: 10.1002/aenm.202103195

Pt on a foreign metal substrate such as Au.[23,24] When Pt grows on an Au substrate at a potential that allows the UPD of H, a layer of H atoms binds strongly to the Pt sites, which leaves the Au surface as the only accessible sites for the deposition of Pt atoms. These techniques make the growth of Pt controllable and, therefore, offer opportunities for the construction of isolated Pt single atoms by controlling the extent of the reaction. However, these electrochemical processes occur on an electrode, rather than in a bulk. Therefore, it is difficult to scale up these syntheses for mass production of the single-atom noble metal catalysts.

In this work, we report a novel ligand-mediated self-terminating growth mechanism in a bulk wet-chemical system for reliably fabricating isolated single atoms of Pt on Au nanoparticles toward enhanced electrocatalytic formic acid oxidation activity. The key is to introduce the ligand of sulfite (SO_3^{2-}) into the growth system, which adsorbs strongly at Pt sites but weakly at Au sites. Because the deposition of a Pt adatom at a preexisting Pt site involves the desorption of a preadsorbed SO_3^{2-} ligand from the Pt site, the formation of Pt–Pt bonds encounters a high energy barrier, making it an energetically unfavorable process, compared with the formation of Au–Pt bonds. In this way, the growth of Pt adatoms at Pt sites is self-terminated, leading to a progressive growth of Pt single atoms, ensembles, and eventually a full monolayer of Pt on the Au substrate. As a result, Pt single atoms can be grown on Au nanoparticles at a relatively high loading (up to 26% coverage of Pt on Au). The resulting single-atom Pt catalyst showed an excellent FAOR activity of 38.6 A mg_{Pt}^{-1} in 0.5 M H_2SO_4 + 0.25 M HCOOH at 0.6 V versus a reversible hydrogen electrode (RHE), which is ≈370 times higher than that of the commercial Pt/C. We believe the ligand-mediated self-terminating growth proposed in this work opens new opportunities for the synthesis of noble metal catalysts with controllable ensemble size for a broad range of catalysis for energy conversion.

2. Results and Discussion

2.1. Design of the Ligand-Mediated Self-Terminating Growth

A prerequisite for the reliable construction of single-atom Pt catalysts is that the Pt adatoms need to be grown on a foreign metal substrate, as demonstrated here by Au, rather than on preexisting Pt atoms. Density functional theory (DFT) calculations predict a strong Pt–Pt bond energy (4.67 eV), which is much higher than that of the Au–Pt bond (3.11 eV, Figure S1, Supporting Information). Therefore, Pt prefers to grow on preexisting Pt atoms, forming ensembles or islands. It is difficult to reliably synthesize isolated Pt single atoms by regular methods.

To suppress the formation of Pt ensembles or islands, we here propose a ligand-mediated self-terminating growth mechanism in a wet-chemical system. We expect that the growth mode of Pt on the Au substrate could be effectively modulated by involving the adsorption of a specific ligand of SO_3^{2-} in the crystal growth. To verify this hypothesis, we conducted DFT calculations to examine the thermodynamics of Pt adatom deposition at a preexisting Au or Pt site on an Au(111) substrate in the presence of a SO_3^{2-} ligand (**Figure 1;** more details, Figures S1 and S2, Supporting Information). A simplified two-step process is considered: First, a SO_3^{2-} ligand desorbs from an Au or Pt atom (target site) on an Au(111) substrate. Then, an incoming Pt atom binds the target site via an Au–Pt or Pt–Pt bond, accompanying an adsorption of a new SO_3^{2-} ligand. In the first step, DFT calculations predict a free energy difference of 0.10 and 1.11 eV to desorb SO_3^{2-} from the Au and Pt sites, respectively (Figure S2, Supporting Information). Therefore, the growth of the Pt adatom at a preexisting Pt site is a kinetically unfavorable process, compared with the growth of the Pt adatom at an Au site. In the second step, the Pt ensemble (Pt–Pt–SO_3^{2-}) on the Au(111) substrate possesses a much lower free energy (-4.67 eV) than the isolated Pt atoms on the Au substrate (Au–Pt–SO_3^{2-}) (-4.12 eV). Thus, the formation of Pt ensembles remains a thermodynamically favorable process in the presence of SO_3^{2-}, compared with the formation of isolated Pt atoms on the Au(111) substrate. These DFT predictions confirm that although the formation of Pt ensembles is a thermodynamically favorable process, a large kinetic barrier exits due to the strong adsorption of SO_3^{2-} at the Pt site, which makes it a kinetically unfavorable process. Although the formation of isolated Pt atoms on the Au substrate is a thermodynamically less favorable process, the kinetic barrier is low (close to 0) due to the weak adsorption of SO_3^{2-} at the Au site, making it a kinetically favorable process. Therefore, we predict SO_3^{2-} can significantly change the growth pattern of Pt on the Au substrate, which makes it possible to fabricate single atoms and (sub-)monolayer of Pt on an Au substrate, depending on the extent of the Pt growth.

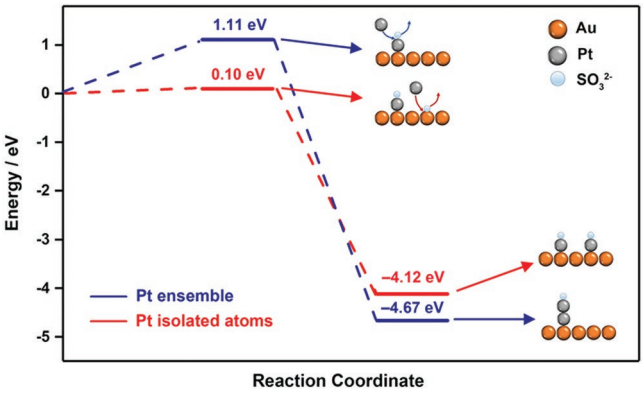

Figure 1. Schematic energy evolution diagram when the ligand of SO_3^{2-} is involved in the growth of a Pt adatom at a preexisting Au site to form an Au–Pt bond and thus Pt single atoms (red line) and at a preexisting Pt site on an Au substrate to form Pt–Pt bond and thus a Pt ensemble/island (blue line).

2.2. Experimental Evidence for the Role of SO_3^{2-} in the Self-Terminating Growth

Under the guidance of DFT calculations, we have successfully achieved the controlled synthesis of Pt single atoms and ensembles on Au nanoparticles by the ligand-mediated self-terminating growth. Ag@Au core–shell nanoplates were employed as the substrates because they possess well-defined (111) terrace facets for the simplified growth environment of Pt.[25] Note

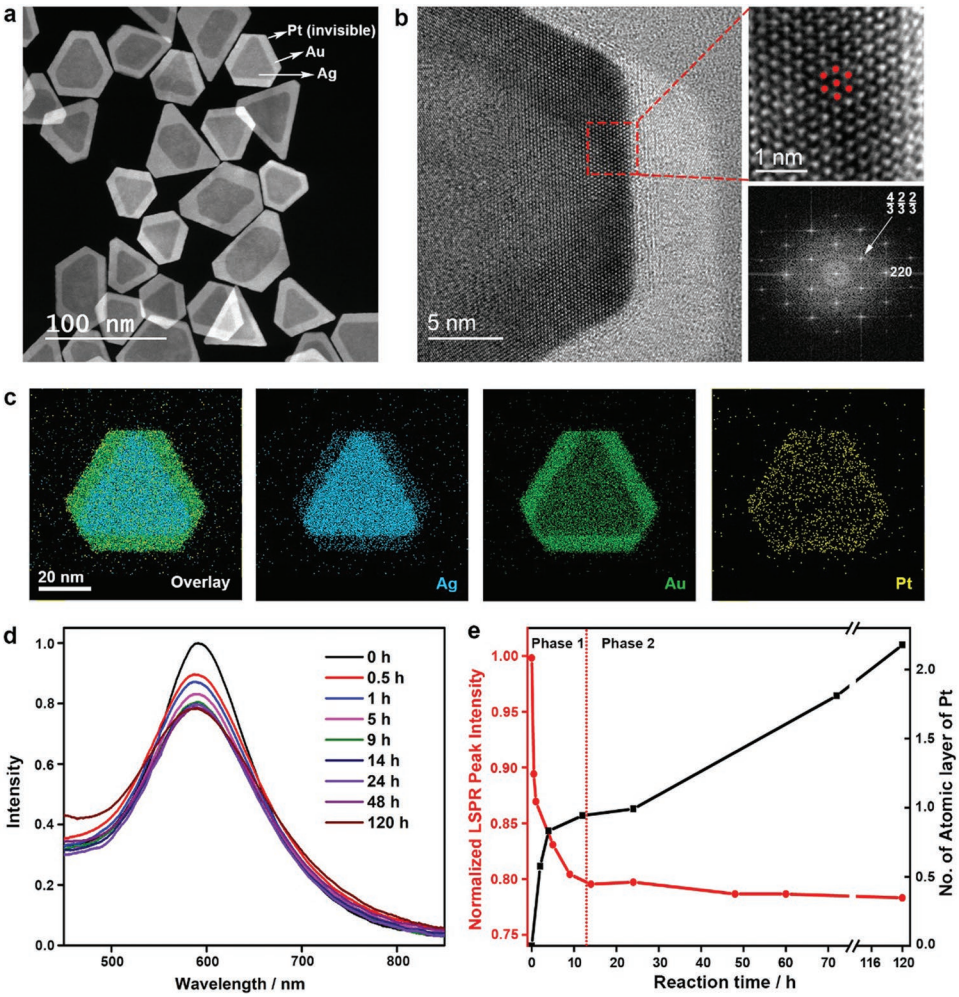

Figure 2. Characterization of the Ag@Au@Pt core–shell nanoplates. a) HAADF-STEM image. b) HRTEM image. Right: An enlarged image, and a Fourier diffractogram. c) EDS elemental mapping of Ag, Au, and Pt in a nanoplate. d) Extinction spectra of the Ag@Au@Pt nanoplates obtained at different reaction time (Pt growth solution, 4 mL). e) Plots of the intensity of the extinction peaks (according to the UV–vis spectra) and the number of the atomic layers of Pt (according to the ICP-MS results) against the reaction time.

that the Ag core does not impose significant influence on the catalytic activity of the Pt sites on the outer Au surface (control experimental results, Figure S3, Supporting Information). The samples are denoted as Ag@Au@Pt_{nL} (n = 0.17, 0.26, 0.43, 0.61, 1.12, and 1.30), where n represents the number of atomic layers (or surface coverage if $n < 1$) of Pt on the Au substrate (calculation details, Figure S4 and Table S1 Supporting Information). **Figure 2**a,b shows a typical high-angle annular dark-field scanning transmission electron microscopy (HAADF-STEM) image and a high-resolution transmission electron microscopy (HRTEM) image of the Ag@Au@$Pt_{0.26L}$ nanoplates (surface coverage by Pt: 26%) (more TEM images, Figures S5 and S6, Supporting Information). The nanoplates expose (111) facets on the basal planes, as confirmed by the atomic arrangement with a threefold symmetry and more unambiguously by the Fourier diffractogram. Diffractions of 1/3(422) in the Fourier diffractogram can be attributed to the stacking faults in the nanoplates.[26] Although the Au/Ag boundary can be clearly observed, the Au/Pt boundary is difficult to be distinguished due to the close atomic numbers of the two elements. The Pt atoms could not be detected by other techniques such as X-ray diffraction (XRD) (Figure S7, Supporting Information). However, the presence of Pt on the Au substrate can be clearly confirmed by the energy-dispersive X-ray spectroscopy (EDS) elemental mapping, showing a homogeneous distribution of Pt on the whole surface of the nanoplate (Figure 2c).

The growth process of the Pt atoms on the Ag@Au nanoplates was investigated to validate the self-terminating growth involved in this synthesis. We first monitored the growth of Pt on the Ag@Au nanoplates by UV–vis spectroscopy, considering that the deposition of plasmonically inactive Pt on the Ag@Au nanoplates significantly alters their localized surface plasmon resonance (LSPR) properties (Figure 2d,e). In the first 14 h of a typical synthesis, the intensity of the LSPR band of the nanoplates dropped very quickly, suggesting a rapid growth of Pt on the nanoplates (phase 1). Subsequently, the LSPR band became stable, indicating a dramatically decreased or virtually terminated growth of Pt on the Ag@Au nanoplates (phase 2). The number of atomic layers (or surface coverage) of Pt on the Au substrate can also be calculated by inductively coupled plasma

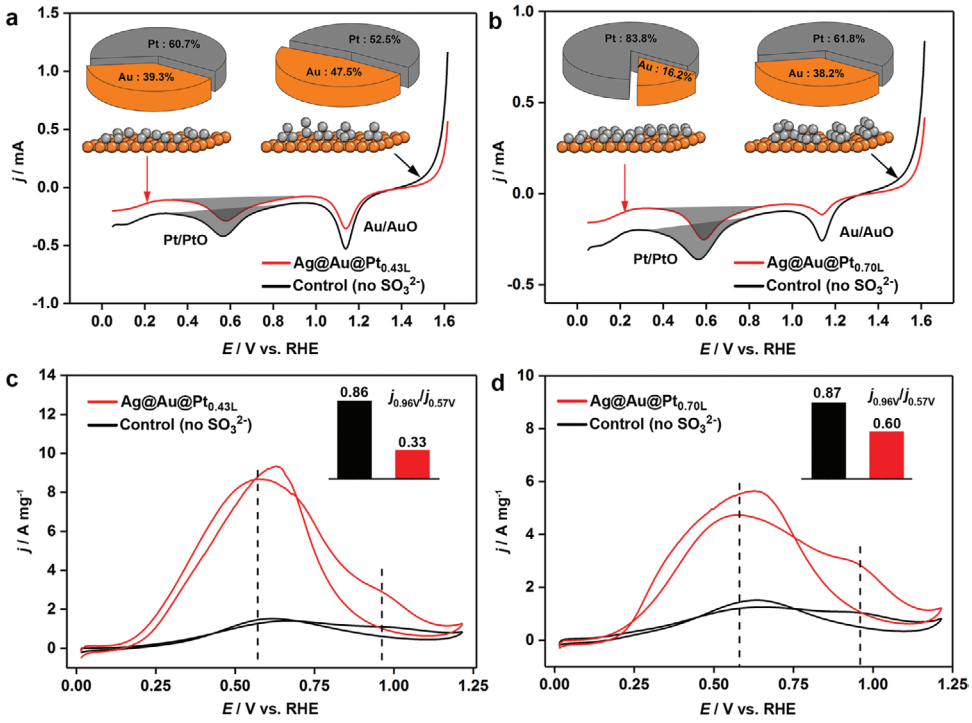

Figure 3. Electrochemical analysis of Pt atoms and ensembles on the Ag@Au nanoplates. a,b) CV curves (cathodic branch) of the Ag@Au@Pt_{nL} (n = 0.43 and 0.70) nanoplates and their counterparts synthesized in the absence of SO_3^{2-} (control samples). The CV curves were recorded in N_2-saturated 0.5 M H_2SO_4 at a scan rate of 50 mV s^{-1}, normalized to the area of PtO reduction peak. Pie charts show the area ratios of the PtO/AuO reduction peaks. c,d) CV curves of the Ag@Au@Pt_{nL} (n = 0.43 and 0.70) nanoplates and the control samples in N_2-saturated 0.5 M H_2SO_4 + 0.25 M HCOOH at a scan rate of 50 mV s^{-1}, normalized to the Pt mass. Insets show the ratios of the current densities at 0.96 and 0.57 V as a descriptor for the degree of CO poisoning in the FAOR.

mass spectrometry (ICP-MS) elemental analysis of the intermediates obtained at different stages of the synthesis (Figure 2e, Table S2, Supporting Information). The two-phase growth of Pt on the Au surface becomes much clearer: The coverage of Pt on the Au substrate increases rapidly to 94% (number of the atomic layer, 0.94, close to a full monolayer) in the first 12 h (phase 1). After that, the growth of Pt dramatically slows down, which requires up to 5 days (≈120 h) to deposit a second layer of Pt on the nanoplates (phase 2). The two-phase growth of Pt on the Ag@Au nanoplates confirms the self-terminating growth: The growth of Pt on an Au substrate is a kinetically favorable and thus quicker process than the growth of Pt on a Pt substrate, due to the difference in the adsorption energy of SO_3^{2-} on these sites. After a full layer of Pt atoms are formed on the Au substrate, the growth becomes a kinetically unfavorable, and therefore slow or literally terminated, process.

We further verified the role of the SO_3^{2-} ligand in the self-terminating growth mechanism by electrochemical techniques (**Figure 3**). Two samples obtained from this synthesis (Ag@Au@Pt_{nL}, n = 0.43 and 0.70) were analyzed, in comparison with their counterparts obtained from a synthesis without SO_3^{2-} (control samples, Figure S8, Supporting Information). The Ag@Au@Pt_{nL} nanoplates and the control samples contain almost the same molar fraction of Pt, according to the ICP-MS. First, cyclic voltammetry (CV) of the nanoplates was measured in N_2-saturated 0.5 M H_2SO_4 (Figure 3a,b). The cathodic peaks at ≈1.14 and ≈0.57 V versus RHE can be ascribed to the reduction of surface AuO and PtO species, respectively. Although the peak areas are sensitive to the potential range and the scan rate in the analysis, they can serve as a rough measure of the exposure of the respective species on the surface, given constant experimental conditions. The proportions of Pt exposed on the surface of the Ag@Au@$Pt_{0.43L}$ nanoplates (Pt%, 3.23%) and the control sample (Pt%, 3.93%) were measured to be 60.7% and 52.5%, respectively. Albeit close Pt fractions in these samples, the Ag@Au@$Pt_{0.43L}$ nanoplates show much higher portion of Pt exposing on the surface than the control sample. Similarly, the Ag@Au@$Pt_{0.70L}$ nanoplates (Pt%, 5.32%) showed much higher exposure of Pt (83.8%) on the surface than their counterparts synthesized without SO_3^{2-} (Pt%, 5.23%; exposure of Pt, 61.8%). Therefore, the presence of SO_3^{2-} in the synthesis greatly reduces the exposure of Au and increases the exposure of Pt on the surface, well agreeing with our hypothesis on the self-terminating growth mechanism, i.e., SO_3^{2-} makes Pt more inclined to grow at Au sites to form single or (sub)monolayer Pt atoms rather than at Pt sites to form Pt islands.

We then employed the electrochemical FAOR to verify the different forms of Pt on the Ag@Au@Pt nanoplates synthesized with and without SO_3^{2-} (Figure 3c,d). The basis of this analysis is that the reaction path of the FAOR is sensitive to the ensemble size of Pt (a scheme, Figure S9, Supporting Information). [7,8] The current densities at 0.96 and 0.57 V versus RHE were extracted from the anodic branch of the CV curves in the FAOR. The former can be ascribed to the oxidation of the CO intermediate

produced via the indirect path of the FAOR, and the latter mainly describes the contribution from the direct path of the FAOR. Therefore, the ratio of the current densities at the two potentials ($j_{0.96\ V}/j_{0.57\ V}$) can be employed as a descriptor for the degree of the CO poisoning and thus the abundance of the Pt ensembles on the surface of the catalysts. The $j_{0.96\ V}/j_{0.57\ V}$ values of the Ag@Au@$Pt_{0.43\ L}$ nanoplates and the corresponding control sample are 0.33 and 0.86, respectively, and those of the Ag@Au@$Pt_{0.70L}$ nanoplates and the corresponding control sample are 0.60 and 0.87, respectively. It is inferred that the FAOR with the Ag@Au@$Pt_{0.43L}$ catalyst proceeds mainly via the direct path without producing substantial CO intermediates ($j_{0.96\ V}/j_{0.57\ V}$, 0.33), confirming that Pt exists mainly as isolated single atoms. With increasing coverage of Pt from 43% to 70%, the direct path of the FAOR still dominates. However, Pt ensembles emerge, causing increasing CO poisoning ($j_{0.96\ V}/j_{0.57\ V}$, 0.60). In clear contrast, the FAOR with the catalysts synthesized without SO_3^{2-} shows low activities with severe CO poisoning ($j_{0.96\ V}/j_{0.57\ V}$, 0.86 and 0.87), which suggests that Pt ensembles are the main form of Pt at both loadings investigated. These results again verify the critical role of SO_3^{2-} in triggering the self-terminating growth mechanism and controlling the ensemble size of Pt on the Au substrate.

2.3. Electrocatalytic Performance of the Catalysts in the FAOR

Thanks to the ligand-mediated self-terminating growth mechanism, Pt can be grown on Au nanoparticles in a wet-chemical synthesis in a highly controllable layer-by-layer manner. By controlling the extent of the Pt growth, single atoms and ensembles of Pt can be reliably obtained according to the need of specific applications. Herein, we show that single-atom Pt catalysts can be synthesized at a relatively high Pt loading on Au nanoparticles for remarkable catalytic activities in the FAOR. Note that a bare Au surface is not active in the electrocatalytic FAOR (Figure S10, Supporting Information). The catalytic formic acid oxidation activities of the Ag@Au@Pt_{nL} nanoplates were measured by CV in 0.5 M H_2SO_4 + 0.25 M HCOOH (**Figure 4**a,b; three parallel experiments, Figure S11, Supporting Information). The commercial Pt/C was employed as a benchmark for comparison. With decreasing atomic layers (or surface coverage) of Pt from 1.30 to 0.17, the ensemble size of Pt is decreasing, which leads to significant changes to the electrocatalytic properties of the Ag@Au@Pt_{nL} nanoplates.

First, the CO oxidation peak at ≈0.96 V versus RHE is obvious when the atomic layer of Pt is in the range of 1.30–0.43 and becomes undiscernible when the atomic layer of Pt is 0.26 and fewer, suggesting the shift of the reaction path from the indirect path to the direct path. With decreasing atomic layers of Pt on the Au substrate, the $j_{0.96\ V}/j_{0.57\ V}$ values decrease continuously, confirming a decreasing degree of CO poisoning in the FAOR due to shift of the reaction path (Figure 4b). It is inferred that Pt exists as ensembles in Ag@Au@Pt_{nL} (n = 0.43, 0.61, 1.12, and 1.30) and transforms into isolated single atoms in Ag@Au@Pt_{nL} (n = 0.26 and 0.17). To further characterize the ensemble size of Pt, we examined the catalytic activities of these

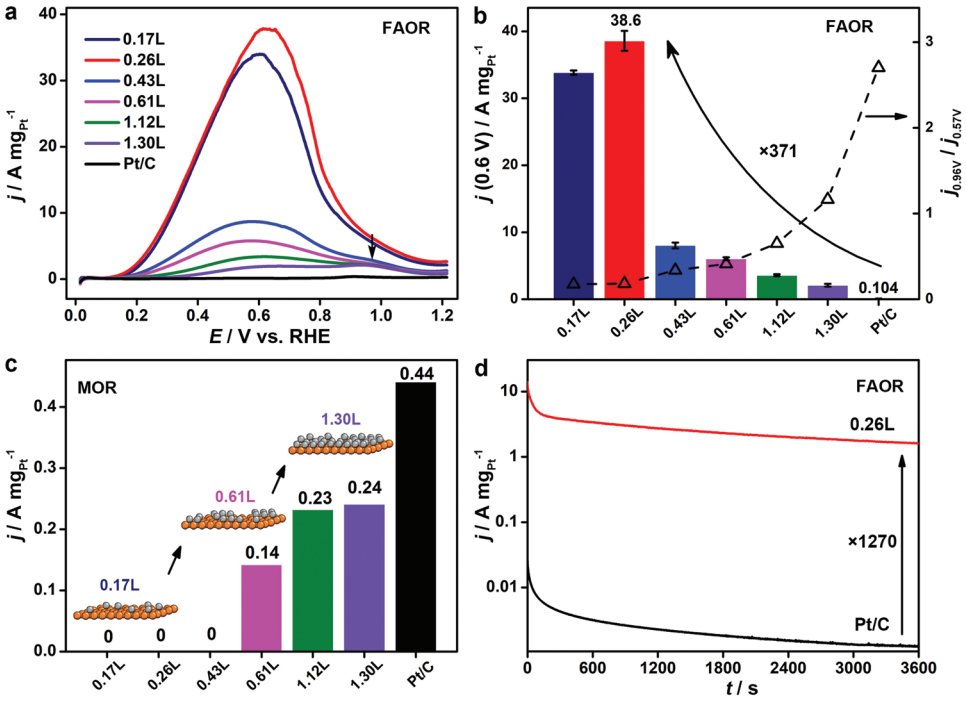

Figure 4. Electrocatalytic performance of the Ag@Au@Pt_{nL} nanoplates and the commercial Pt/C. a) CV curves of the catalysts in N_2-saturated 0.5 M H_2SO_4 + 0.25 M HCOOH at a scan rate of 50 mV s^{-1} (FAOR). The arrow indicates the CO oxidation peak due to the indirect path of the FAOR. b) Left axis: Comparison of the mass activities of the catalysts in the FAOR. Error bars indicate the standard deviations from 3 parallel experiments. Right axis: $j_{0.96\ V}/j_{0.57\ V}$ values for the catalysts as a measure of the CO poisoning in the FAOR. c) Comparison of the mass activities of the catalysts in N_2-saturated 0.5 M H_2SO_4 + 1 M CH_3OH at a scan rate of 50 mV s^{-1} (MOR). d) Chronoamperometric i–t curves of the Ag@Au@$Pt_{0.26L}$ nanoplates and the commercial Pt/C at 0.345 V versus RHE in an FAOR.

catalysts in the methanol oxidation reaction (MOR), which is also an ensemble-size-sensitive reaction occurring mainly at Pt ensembles of 3–4 contiguous Pt atoms (Figure 4c and Figures S12 and S13, Supporting Information).[5,6,9] The Ag@Au@Pt_{nL} nanoplates are active for the MOR when the atomic layer of Pt is 0.61 and higher but completely lose their activities when the atomic layer of Pt decreases to 0.43 and fewer. Combining both the FAOR and MOR results, we can conclude that the main forms of Pt are isolated single atoms, ensembles of 3–4 atoms, and larger ensembles when the atomic layers of Pt are 0.17–0.26, 0.43, and 0.61–1.30, respectively. We also investigated the electrocatalytic properties of the Ag@Au@Pt_{nL} nanoplates in oxygen reduction reaction (ORR), which is also an ensemble-sensitive reaction (Figure S14, Supporting Information).[27–29] The ORR usually follows a two-electron path ($O_2 + 2H^+ + 2e \rightarrow H_2O_2$) at Pt single atoms and a four-electron path ($O_2 + 4H^+ + 4e \rightarrow 2H_2O$) at Pt ensembles. Our results show that the ORR proceeds via a four-electron path with the Ag@Au@$Pt_{1.30L}$ nanoplates and mainly a two-electron path with the Ag@Au@$Pt_{0.26L}$ nanoplates, confirming that Pt exists on the nanoplates in the form of ensembles and single atoms, respectively. It is worth noting that single atoms of Pt have been obtained with Ag@Au@$Pt_{0.26L}$ (surface coverage of Pt on Au, 26%), which is a significantly higher loading of Pt than single-atom Pt catalysts synthesized by a conventional method as reported in the literature (typically < 0.1 L),[18] highlighting the superiority of the self-terminating growth mechanism in reliably regulating the growth mode of Pt on the Au substrate.

Second, the catalytic FAOR activities are low when atomic layer of Pt is in the range of 1.30–0.43 and become extremely high when the atomic layer of Pt is 0.26 and fewer (Figure 4a,b). The exceptional catalytic activities of the Ag@Au@Pt_{nL} (n = 0.26 and 0.17) catalysts can be largely attributed to the shift of the reaction path and therefore effective suppression of the CO poisoning of the catalysts. The activity values of the two samples are very close, showing only a slight difference, which may arise experimentally from the systematic errors in determining the amount of Pt on the electrodes by ICP-MS, especially when these single-atom catalysts with ultralow loadings of Pt are to the analyzed. Specifically, the Ag@Au@$Pt_{0.26L}$ nanoplates show a mass activity of 38.6 A mg_{Pt}^{-1} in the FAOR, which is ≈370 times greater than that of the commercial Pt/C (0.104 A mg_{Pt}^{-1}). We also tested the catalytic performance of the Ag@Au@$Pt_{0.26L}$ nanoplates in N_2-saturated 0.1 M H_2SO_4 + 0.5 M HCOOH (Figure S15, Supporting Information). The mass activity was 69.3 A mg_{Pt}^{-1}, which places the nanoplates among the best catalysts reported so far (Table S3, Supporting Information).[18,29–37] It is worth noting that the Ag@Au@$Pt_{0.26L}$ nanoplates also show a high mass activity normalized to the total mass of the metals (0.811 A $mg_{Au+Ag+Pt}^{-1}$), which is 7.8 times greater than that of the commercial Pt/C, suggesting a high potential of these catalysts in practical applications (Figure S16, Supporting Information).

The single-atom Pt catalysts also show high durability in the electrocatalysis (Figure 4d and Figure S17, Supporting Information). In a typical chronoamperometric *i–t* test, the Ag@Au@$Pt_{0.26L}$ nanoplates retained a high current density after 3600 s, which was 1270 times greater than that of the commercial Pt/C (Figure 4d). The high catalytic durability can be attributed to the reliable isolation of the single Pt atoms on the Au substrate, which allows the FAOR to proceed only via the direct path so that the CO poisoning of the catalysts has been effectively suppressed. In addition, the morphology, electronic structure, and composition of the Ag@Au@$Pt_{0.26L}$ nanoplates have been well retained during the electrocatalysis, which also contributes to the high catalytic durability (Figures S18–S20, Supporting Information).

3. Conclusion

In summary, we have developed a novel ligand-mediated self-terminating growth strategy in a wet-chemical system for controlling the ensemble size of Pt atoms on an Au substrate. The key to the synthesis is to take advantage of the huge difference between the adsorption energies of SO_3^{2-} at Au and Pt sites. With SO_3^{2-}, the growth of a Pt adatom at a Pt site needs to overcome a large energy barrier and therefore becomes kinetically unfavorable, compared with the growth of the Pt adatom at an Au site. As a result, the growth of the Pt atoms occurs preferentially at the Au sites until a full layer of Pt is formed on the Au substrate. By controlling the extent of the Pt growth, isolated single atoms of Pt have been reliably deposited on Ag@Au core–shell nanoplates at a surface coverage of up to 26% before the emergence of ensembles, which is a significantly higher loading than the catalysts obtained from conventional syntheses. The formation of isolated single atoms and ensembles of Pt has been examined and confirmed electrochemically by FAOR, MOR and ORR. The resulting Ag@Au@Pt_{nL} nanoplates show record-high catalytic activities in the electrocatalytic FAOR, benefiting from the reliable construction of the single Pt atoms that allow the FAOR to proceed via the direct path without involving the poisoning CO intermediates. We believe the ligand-mediated self-terminating growth mechanism developed in this work is general and potentially applicable in synthesizing a wide range of noble metal catalysts with tailored ensemble sizes for energy conversion applications.

4. Experimental Section

Synthesis of Ag@Au@Pt_{nL} Nanoplates: First, a growth solution of Pt was prepared by mixing 0.1 mL of H_2PtCl_6 (0.1 M), 3 mL Na_2SO_3 (0.01 M), and 0.24 mL NaOH (0.2 M) in 4.66 mL H_2O and allowed to be aged for 12 before use. In a typical synthesis of Ag@Au@Pt_{nL} nanoplates, 0.2–4.0 mL of Pt growth solution (Table S1, Supporting Information), 1 mL of PVP (M_w 40000, 5 wt%), 0.4 mL of NaOH (0.5 M), and 0.4 mL of AA were added to H_2O (total volume of the solution, 8 mL). Then, 2 mL of the Ag@Au nanoplates was added to this solution at 60 °C to trigger the seeded growth. The synthesis was allowed to proceed for 14 h to obtain Ag@Au@Pt_{nL} (n = 0.17, 0.26, 0.43, and 0.61) and proceed for 48 h to obtain Ag@Au@Pt_{nL} (n = 1.12 and 1.30). Finally, the Ag@Au@Pt_{nL} nanoplates were collected by centrifugation, washed with H_2O, and redispersed in 1 mL of H_2O.

Electrochemical Measurements: All measurements were taken on a CHI 760e electrochemical workstation (CH Instruments, Inc.) with a three-electrode configuration at 25 °C. A rotating disk electrode (RDE, 0.196 cm^2), a Pt foil (1 cm × 1 cm), and a Ag/AgCl was used as the working, counter, and reference electrodes, respectively. The Ag@Au@Pt_{nL} nanoplates were supported on Vulcan XC-72 carbon and dispersed in a mixture of H_2O/isopropanol/Nafion (5%) = 1:1:0.004 (volume

ratio) to form a homogeneous ink. Then, an ink containing 0.5 µg of Pt (determined by ICP-MS) was dropped and dried on an RDE. Before electrochemical measurements, the sulfite ligands on the catalysts were oxidized to sulfate by 20 cycles of CV in N_2-saturated 0.5 M H_2SO_4 so that the active Pt sites can be exposed for electrocatalysis (Figure S21, Supporting Information). CV curves were collected in either N_2-saturated 0.5 M H_2SO_4 + 0.25 M HCOOH to evaluate the FAOR activity, or in N_2-saturated 0.5 M H_2SO_4 + 1.0 M CH_3OH to evaluate the MOR activity, both in the potential range of 0.015–1.215 V versus RHE at a sweep rate of 50 mV s^{-1}. The catalytic durability of the catalysts in the FAOR was conducted by chronoamperometry in N_2-saturated 0.5 M H_2SO_4 + 0.25 M HCOOH at 0.345 V versus RHE for 3600 s. The CO stripping voltammetry was conducted in 0.5 M H_2SO_4. The electrolyte was first bubbled with CO for 30 min at 0.1 V versus RHE. Then, the gas was changed to N_2 and bubbled for another 30 min. After that, CV was obtained in the potential range of 0.05–1.11 V versus RHE at a sweep rate of 20 mV s^{-1} for 2 cycles. The electrochemically active surface area (ECSA) of the Ag@Au template was estimated by the underpotential deposition (UPD) of Cu in N_2-saturated 0.05 M H_2SO_4 + 0.05 M $CuSO_4$ at a sweep rate of 5 mV s^{-1}, assuming a charge constant of 420 µC cm^{-2}.[20,38]

DFT Calculations: The quantum mechanics (QM) calculations were carried out using the VASP software, version 5.4.4.[39,40] One used the Perdew, Burke, and Ernzerhof (PBE)[41] flavor of DFT with the post-stage DFT-D3 method to correct for London dispersion (van der Waals attraction)[42] with Becke-Johnson damping. The projector augmented wave (PAW)[43,44] method was used to account for core–valence interactions. The kinetic energy cutoff for plane wave expansions was set to 400 eV, and reciprocal space was sampled by the Γ-centered Monkhorst-Pack scheme with a grid of 3 × 3 × 1. The convergence criteria are 1×10^{-5} eV energy differences for solving the electronic wave function. The Methfessel-Paxton smearing of second order with a width of 0.2 eV was applied. All atomic coordinates were converged to within 3×10^{-2} eV $Å^{-1}$ for maximal components of forces. Moreover, one implemented an implicit solvation model (VASPsol)[45,46] that computed the energy of H_2SO_3 and SO_3^{2-} under water solvent.

Characterizations: TEM was performed on a Hitachi HT-7700 at an accelerating voltage of 100 kV. HRTEM and EDS elemental mapping were performed on a JEM-F200-TEM at an accelerating voltage of 200 kV. UV–vis spectra were collected on an Ocean Optics HR2000+ES UV–vis–NIR spectrophotometer with a DH-2000-Bal light source. XRD patterns were recorded on a Rigaku SmartLab powder X-ray diffractometer equipped with Cu Kα radiation. ICP-MS was performed on a PerkinElmer NexION 350D.

Supporting Information

Supporting Information is available from the Wiley Online Library or from the author.

Acknowledgements

M.L. and Z.L. contributed equally to this work. C.G. acknowledges the support by the National Natural Science Foundation of China (22071191), Key Research and Development Program of Shaanxi (2021GXLH-Z022), the Key Scientific and Technological Innovation Team of Shaanxi Province (2020TD-001), the Fundamental Research Funds for the Central Universities, and the World-Class Universities (Disciplines) and the Characteristic Development Guidance Funds for the Central Universities. T.C. was supported by the National Natural Science Foundation of China (21903058), the Natural Science Foundation of Jiangsu Province (BK20190810), and Jiangsu Province High-Level Talents (JNHB-106). The authors thank the Instrument Analysis Center of Xi'an Jiaotong University for partial assistance with the TEM and ICP-MS measurements.

Conflict of Interest

The authors declare no conflict of interest.

Data Availability Statement

Research data are not shared.

Keywords

ensemble size, FAOR, noble metals, self-terminating growth, single atoms

Received: October 14, 2021
Revised: November 4, 2021
Published online: November 17, 2021

[1] H. Wang, J. Chen, Y. Lin, X. Wang, J. Li, Y. Li, L. Gao, L. Zhang, D. Chao, X. Xiao, J. M. Lee, *Adv. Mater.* **2021**, *33*, 2008422.
[2] P. Prabhu, J. M. Lee, *Chem. Soc. Rev.* **2021**, *50*, 6700.
[3] V. Jose, J. Nsanzimana, H. Hu, J. Choi, X. Wang, J. M. Lee, *Adv. Energy Mater.* **2021**, 11, 2100157.
[4] P. Prabhu, V. Jose, J.-M. Lee, *Matter* **2020**, *2*, 526.
[5] S. Park, Y. Xie, M. J. Weaver, *Langmuir* **2002**, *18*, 5792.
[6] J. Kim, C. Jung, C. K. Rhee, T. H. Lim, *Langmuir* **2007**, *23*, 10831.
[7] M. Neurock, M. Janik, A. Wieckowski, *Faraday Discuss.* **2009**, *140*, 363.
[8] N. Kristian, Y. Yan, X. Wang, *Chem. Commun.* **2008**, 353.
[9] A. Cuesta, *J. Am. Chem. Soc.* **2006**, *128*, 13332.
[10] C. Yang, L. Jian, L. Lin, B. Qiao, J. Liu, S. Yang, X. Wang, *ACS Catal.* **2018**, *8*, 859.
[11] Y. Wang, H. Arandiyan, J. Scott, K. F. Aguey-Zinsou, R. Amal, *ACS Appl. Energy Mater.* **2018**, *1*, 6781.
[12] H. Jeong, O. Kwon, B. S. Kim, J. Bae, H. Lee, *Nat. Catal.* **2020**, *3*, 368.
[13] S. Shin, H. Kim, B. Kim, S. J. Sun, H. Jeong, H. Lee, *ChemElectroChem* **2020**, *7*, 3716.
[14] J. Wu, H. Yang, *Acc. Chem. Res.* **2013**, *46*, 1848.
[15] Z. Peng, H. Yang, *J. Am. Chem. Soc.* **2009**, *131*, 7542.
[16] Z. Peng, J. Wu, H. Yang, *Chem. Mater.* **2010**, *22*, 1098.
[17] H. Ataee-Esfahani, L. Wang, Y. Nemoto, Y. Yamauchi, *Chem. Mater.* **2010**, *22*, 6310.
[18] S. Yang, H. Lee, *ACS Catal.* **2013**, *3*, 437.
[19] R. Wang, C. Wang, W. B. Cai, Y. Ding, *Adv. Mater.* **2010**, *22*, 1845.
[20] L. Peng, L. Gan, Y. Wei, H. Yang, J. Li, H. Du, F. Kang, *J. Phys. Chem. C* **2016**, *120*, 28664.
[21] B. I. Podlovchenko, Y. M. Maksimov, K. I. Maslakov, *Electrochim. Acta* **2014**, *130*, 351.
[22] M. Khosravi, M. K. Amini, *Int. J. Hydrogen Energy* **2010**, *35*, 10527.
[23] S. H. Ahn, Y. Liu, T. P. Moffat, *ACS Catal.* **2015**, *5*, 2124.
[24] Y. Liu, D. Gokcen, U. Bertocci, T. P. Moffat, *Science* **2012**, *338*, 1327.
[25] H. Liu, T. Liu, L. Zhang, L. Han, C. Gao, Y. Yin, *Adv. Funct. Mater.* **2015**, *25*, 5435.
[26] V. Germain, J. Li, D. Ingert, Z. L. Wang, M. P. Pileni, *J. Phys. Chem. B* **2003**, *107*, 8717.
[27] S. Yang, J. Kim, Y. J. Tak, A. Soon, H. Lee, *Angew. Chem., Int. Ed.* **2016**, *55*, 2058.
[28] A. von Weber, E. T. Baxter, H. S. White, S. L. Anderson, *J. Phys. Chem. C* **2015**, *119*, 11160.

[29] J. Kim, C. W. Roh, S. K. Sahoo, S. Yang, J. Bae, J. W. Han, H. Lee, *Adv. Energy Mater.* **2018**, *8*, 1701476.
[30] G.-R. Zhang, D. Zhao, Y.-Y. Feng, B. Zhang, D.-S. Su, G. Liu, B.-Q. Xu, *ACS Nano* **2012**, *6*, 2226.
[31] H. Fan, M. Cheng, L. Wang, Y. Song, Y. Cui, R. Wang, *Nano Energy* **2018**, *48*, 1.
[32] F. Li, Y. Ding, Y. Xiao, S. Yin, M. Hu, S. Li, Y. Chen, *J. Mater. Chem. A* **2018**, *6*, 17164.
[33] J. Li, S. Z. Jilani, H. Lin, X. Liu, K. Wei, Y. Jia, P. Zhang, M. Chi, Y. J. Tong, Z. Xi, S. Sun, *Angew. Chem., Int. Ed.* **2019**, *58*, 11527.
[34] J. Jiang, W. Ding, W. Li, Z. Wei, *Chem* **2020**, *6*, 431.
[35] Y. Xie, N. Dimitrov, *Appl. Catal., B* **2020**, *263*, 118366.
[36] H. Shi, F. Liao, W. Zhu, C. Shao, M. Shao, *Int. J. Hydrogen Energy* **2020**, *45*, 16071.
[37] M. Tang, W. Chen, S. Luo, X. Wu, X. Fan, Y. Liao, X. Song, Y. Cheng, L. Li, L. Tan, Y. Liu, Z. Quan, *J. Mater. Chem. A* **2021**, *9*, 9602.
[38] M. Shao, J. H. Odell, S. I. Choi, Y. Xia, *Electrochem. Commun.* **2013**, *31*, 46.
[39] G. Kresse, J. Hafner, *Phys. Rev. B* **1993**, *47*, 558.
[40] G. Kresse, J. Furthmüller, *Phys. Rev. B* **1996**, *54*, 11169.
[41] J. P. Perdew, K. Burke, M. Ernzerhof, *Phys. Rev. Lett.* **1996**, *77*, 3865.
[42] S. Grimme, J. Antony, S. Ehrlich, H. Krieg, *J. Chem. Phys.* **2010**, *132*, 154104.
[43] P. E. Blöchl, *Phys. Rev. B* **1994**, *50*, 17953.
[44] G. Kresse, D. Joubert, *Phys. Rev. B* **1999**, *59*, 1758.
[45] M. Fishman, H. L. Zhuang, K. Mathew, W. Dirschka, R. G. Hennig, *Phys. Rev. B* **2013**, *87*, 245402.
[46] K. Mathew, R. Sundararaman, K. Letchworth-Weaver, T. A. Arias, R. G. Hennig, *J. Chem. Phys.* **2014**, *140*, 084106.